Superconductor Science and Technology

PAPER

Promising effects of a new *hat structure* and double metal ring for mechanical reinforcement of a REBaCuO ring-shaped bulk during field-cooled magnetisation at 10 T without fracture

To cite this article: H Fujishiro *et al* 2019 *Supercond. Sci. Technol.* **32** 065001

IOP Publishing Superconductor Science and Technology
Supercond. Sci. Technol. **32** (2019) 065001 (12pp) https://doi.org/10.1088/1361-6668/ab0bed

Promising effects of a new *hat structure* and double metal ring for mechanical reinforcement of a REBaCuO ring-shaped bulk during field-cooled magnetisation at 10T without fracture

H Fujishiro[1], T Naito[1], Y Yanagi[2], Y Itoh[2] and T Nakamura[3]

[1] Department of Physical Science and Materials Engineering, Faculty of Science and Engineering, Iwate University, 4-3-5 Ueda, Morioka 020-8551, Japan
[2] IMRA Material R&D Co., Ltd, 2-1 Asahi-machi, Kariya 448-0032, Japan
[3] RIKEN, 2-1 Hirosawa, Wako 351-0198, Japan

E-mail: fujishiro@iwate-u.ac.jp

Received 2 December 2018, revised 20 February 2019
Accepted for publication 1 March 2019
Published 23 April 2019

Abstract

We have investigated a new reinforcement *hat structure* for a RE-Ba-Cu-O (REBaCuO, RE: rare earth element or Y) ring-shaped bulk superconductor (ring bulk) shrink-fitted with a double Al alloy ring and set on the cold stage of a cryogenic refrigerator prior to field-cooled magnetisation (FCM). With the hat structure, a ring bulk having an outer diameter of 64 mm, inner diameter of 40 mm, and height of 20.5 mm achieved a trapped field as high as 6.8 T at 50 K during FCM with an applied magnetic field at $B_{app} = 10$ T without fracture; a similar ring bulk without the hat structure broke during FCM at $B_{app} = 8.8$ T. Using a numerical simulation for electromagnetic and mechanical properties, the potential benefit of the hat structure was confirmed. The magnetic field dependence of the average critical current density $J_c(B)$ of the ring bulk used in the simulation was determined by experimental results of time step dependence of the trapped field B_z at the bulk centre. As a result, the total hoop stress σ_θ^{total} in the ring bulk including the resulting stress of cooling from 300 K to 50 K and subsequent FCM at $B_{app} = 10$ T is lower than the fracture strength of a typical Ag-doped REBaCuO bulk material. The effect of double Al alloy ring reinforcement was also analysed using a numerical simulation and compared with that of the conventional single Al alloy ring reinforcement. These results suggest that the double ring provides only a limited benefit, whereas the hat structure is fairly effective in reducing the electromagnetic hoop stress during FCM at $B_{app} = 10$ T. Using this reinforcement method, a 400 MHz (9.4 T) nuclear magnetic resonance bulk magnet system could be realised.

Keywords: REBaCuO superconducting bulk, field cooled magnetization, trapped field, electromagnetic hoop stress, mechanical reinforcement, numerical simulation

(Some figures may appear in colour only in the online journal)

1. Introduction

It is important to enhance the trapped magnetic field in RE-Ba-Cu-O (REBaCuO, RE: rare earth element or Y) superconducting ring-shaped bulks (ring bulks) because the high-field trapped field magnet is capable of generating several Tesla. Although the trapped field estimated from its critical current density $J_c(B, T)$ could theoretically be over 30 T at 29 K [1], the mechanical strength of the brittle ceramic material restricts the maximum trapped field experimentally. A

trapped field of 16 T has been achieved at 24 K in an Ag- and Zn-doped YBaCuO disc bulk pair reinforced by austenite Cr–Ni steel tubes [2], and a trapped field of 17.24 T has been achieved at 29 K in a YBaCuO disc bulk pair by mechanical reinforcement of resin impregnation and carbon fibre wrapping [1]. To date, the highest trapped field of 17.6 T has been achieved at 26 K in a GdBaCuO disc bulk pair reinforced by shrink-fit stainless steel [3]. A REBaCuO ring-shaped bulk superconductor is useful for practical applications such as nuclear magnetic resonance (NMR) spectrometers and magnetic resonance imaging (MRI) equipment [4–6]. Trapped field enhancement in the ring bulk of an NMR/MRI system is an ongoing challenge for improving resolution; a trapped field of as high as 10 T is necessary to realise a 400 MHz (9.4 T) NMR bulk magnet system.

It should be noted that the above analytical investigations of mechanical properties were reported only for disc- and ring-shaped bulks of infinite height during field-cooled magnetisation (FCM) or zero-field-cooled magnetisation [7–9]; the results were primarily based on Bean's critical state model with constant J_c characteristics independent of magnetic field. Huang *et al* investigated the magnetostriction of a superconducting disc or ring of finite height using the finite element method (FEM), in which Bean's model and a uniform applied field from an infinite magnetising solenoid coil were assumed [10]. Furthermore, there have been no numerical simulations of the reinforcement effect of the metal ring fitting on the mechanical stresses in the superconducting disc- and ring-shaped bulks during FCM and the cooling process, except for the relevant work by Johansen *et al* [11].

Therefore, we have reported numerical simulation results of the mechanical stress behaviours in REBaCuO ring and disc bulks of finite height and the metal ring reinforcement during FCM [12–14], and we have also proposed a new reinforcement method to prevent bulk failure [15, 16]. The following points have been clarified so far.

(1) In REBaCuO ring bulks of finite height reinforced by a metal (Al alloy or stainless steel) ring, the compressive stress is non-uniformly applied to the ring bulk during the cooling process from room temperature to the operating temperature of FCM. More specifically, the applied compressive stress is reduced at the periphery of the bulk surface and, in some cases, changes to tensile stress because a larger thermal contraction of the metal ring takes place along both radial and height directions relative to that of the bulk [12].
(2) The electromagnetic hoop stress $\sigma_\theta^{\mathrm{FCM}}$ during FCM achieves a maximum at the inner peripheral surface of the ring bulk, which is larger than that for a disc bulk with an identical outer diameter and height [12, 13].
(3) The thermal compressive stress $\sigma_\theta^{\mathrm{cool}}$ increases in the ring bulk during the cooling process from room temperature to operating temperature, and $\sigma_\theta^{\mathrm{FCM}}$ during FCM decreases with the increasing width of the metal ring w_r. As a result, the total hoop stress $\sigma_\theta^{\mathrm{total}}$ $(= \sigma_\theta^{\mathrm{cool}} + \sigma_\theta^{\mathrm{FCM}})$ can be reduced at the innermost surface of the ring bulk [14].
(4) To restrict the reduction of $\sigma_\theta^{\mathrm{cool}}$ on the ring bulk surface, a new numerically simulated reinforcement structure has been proposed, in which thick metal plates are tightly moulded above and below the metal ring. As a result, a 400 MHz (9.4 T) NMR bulk magnet can be realised without fracture [15].
(5) The mechanical strain has been directly measured on a ring bulk surface during the cooling process and FCM using a strain gauge, verifying that the simulation results qualitatively reproduce the experimental results [16].

For the numerical models used in the simulation, we assumed that there was no slippage at the interface between the outer ring bulk surface and the inner metal ring surface. Such assumptions of mechanical behaviour and associated numerical results should be validated and compared with actual experimental results; previous investigations have been typically performed by simulation only. We performed several FCM experiments with an applied magnetic field B_{app} of 5–7 T at 50 K for REBaCuO ring bulks reinforced by a metal (Al alloy or stainless steel) ring of identical height; a mechanical fracture frequently occurred. Although we have proposed the new reinforcement method to prevent this ring bulk fracture [15], actual experimental confirmation has not been performed.

In this paper, we report the results of FCM experiments for a B_{app} of up to 10 T at 50 K using a new reinforcement hat structure for EuBaCuO ring bulk reinforced by a double Al alloy ring and set on the cold stage of a cryogenic refrigerator. The EuBaCuO ring bulk with this reinforcement can achieve higher trapped field and magnetic field homogeneity with low relative magnetic permeability ($\mu_r = 1.0013$), which is preferable for NMR/MRI bulk magnets [5]. As a result, the experimental FCM procedure at $B_{\mathrm{app}} = 10$ T succeeded without fracture, and a trapped field of 6.8 T was safely achieved at the centre of the ring bulk. We analysed the effects of the double Al alloy ring reinforcement and the hat structure using numerical simulation and compared them with those of single Al alloy ring reinforcement as well as those without the hat structure.

2. Experimental procedure

Two EuBaCuO ring-shaped bulks were prepared: *bulk-A* with an outer diameter (OD) of 64 mm, inner diameter (ID) of 32 mm, and height (ht) of 13 mm, and *bulk-B* with 64 mm OD, 40 mm ID, and 20.5 mm ht; both were fabricated by Nippon Steel & Sumitomo Metal, Japan. The double Al alloy ring structure for each ring bulk was applied by the following process. First, the inner Al alloy ring (A7075-T6) with 1.5 mm in width (67 mm OD and 64.1 mm ID for both bulk-A and bulk-B) was moulded using 0.05 mm thick Stycast™ 1266 resin at room temperature. Second, the outer Al alloy ring (A7075-T6) 3.4 mm wide (74 mm OD and 66.70 mm ID for bulk-A, and 74 mm OD and 66.84 mm ID for bulk-B, which is slightly smaller than the OD of the inner ring) was

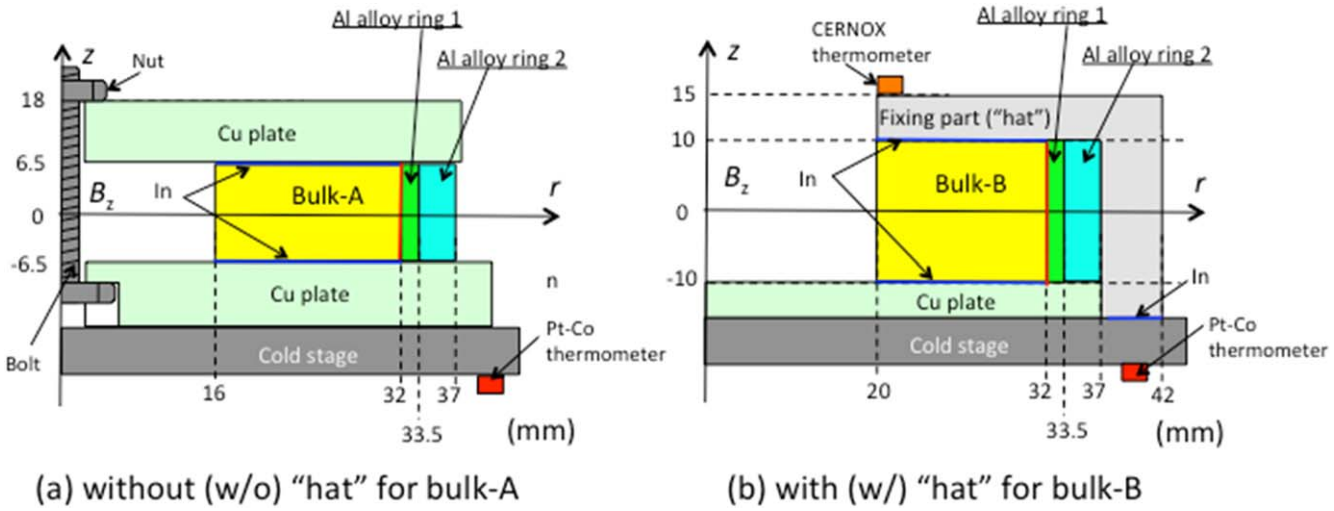

Figure 1. The experimental setup of (a) bulk-A and (b) bulk-B on the cold stage of the cryogenic refrigerator during FCM. Bulk-A was sandwiched by Cu plates using a nut and bolt, and the bottom Cu plate was thermally connected to the cold stage. Bulk-B was mechanically and thermally fixed to the cold stage using a reinforcement hat structure.

mechanically pressed into the outer periphery of the inner ring using a tapered die. The double ring reinforcement was expected to add an initial compressive stress before the shrink-fit process, which is a new method to reinforce the bulk. The double ring reinforcement is suitable for practical applications because it shows a comparable effect to that of a thicker single ring, and the ring bulk can be safely magnetised in a magnet bore with limited size.

Figure 1(a) shows the experimental setup for bulk-A reinforced by the double Al alloy ring set on the cold stage of a cryogenic refrigerator. Bulk-A was sandwiched by thick Cu plates with 0.1 mm thin indium (In) sheets using a nut and bolt, and the bottom Cu plate was thermally connected to the cold stage. Figure 1(b) shows the experimental setup for bulk-B reinforced with the double Al alloy ring. Bulk-B was thermally and mechanically connected to the cold stage of the cryogenic refrigerator using the hat structure (74.26 mm ID, 84 mm OD, and 5 mm thickness of the upper plate), also made of Al alloy, by the insertion of an In sheet. The temperature of each ring bulk was controlled by a Pt–Co thermometer attached to the bottom surface of the cold stage. In the FCM process, bulk-A was cooled to the magnetising temperature of $T_s = 50$ K under the applied field of $B_{app} = 7.3$, 8.3, and 8.8 T using a cryocooled superconducting solenoid magnet (JASTEC JMTD-10T100). The external field was then decreased linearly at -0.222 T min^{-1} down to zero. Bulk-B with the hat structure was also cooled to $T_s = 50$ K under the applied field of $B_{app} = 7.3$, 8.3, 8.8, 9.4, and 10 T, and the external field was decreased linearly at the same ramp rate down to zero.

The time step (*TS*) of the decline of the magnetic field during FCM is defined as $TS = 10(B_{app} - B_{ex})/B_{app}$, where B_{ex} is the actual applied field at the bulk centre. The *TS* dependence of the local field $B_z(t)$ along the z-direction was measured at the centre of the bulk annuli ($z = r = 0$) using a Hall sensor (F. W. Bell, BHA921) for each case. For bulk-B, the *TS* dependence of temperature $T(t)$ was also measured by a CERNOX^{TM} thermometer on the top of the hat structure.

3. Numerical simulation framework

To understand the effects of the hat structure and double ring reinforcement, numerical simulation models were constructed. Figure 2 shows the cross-sectional view of the numerical model. Based on the experimental setup of bulk-B shown in figure 1(b), we constructed a three-dimensional finite element model for a REBaCuO ring-shaped bulk (64 mm OD, 40 mm ID, and 20 mm ht). In the previous section, bulk-B was experimentally reinforced by a double Al alloy ring using uniaxial pressing. Because it is difficult to reproduce the mechanical pressing process of the outer ring (Al alloy ring 2), the outer ring was instead heated to 540 K in the numerical simulation and then smoothly inserted into the outer periphery of the inner ring (Al alloy ring 1), and then cooled to 300 K, as shown in figure 2(a). This numerical assumption seemed to reproduce the double ring effect for bulk-B. To verify the effect of the double Al alloy ring on mechanical reinforcement, the ring bulk was also mounted inside a single Al alloy ring of 5 mm in width (74 mm OD, 64.1 mm ID, and 20 mm ht) using an epoxy resin at 300 K, as shown in figure 2(b).

The REBaCuO ring bulk reinforced by the double or single Al alloy ring as shown in figures 2(a) and (b), respectively, was connected to a Cu plate set on the cold stage of the cryogenic refrigerator using an In sheet with 0.1 mm in thickness; it was then reinforced by the hat structure as shown in figure 2(c). The numerical simulation of the cooling process from 300 to 50 K and that of the subsequent FCM using a solenoid coil (170 mm OD, 120 mm ID and 200 mm ht) were performed. In the experimental setup of the ring bulk with the hat structure as shown in figure 1(b), the gap between the OD of the outer Al alloy ring (74.0 mm) and ID of the hat

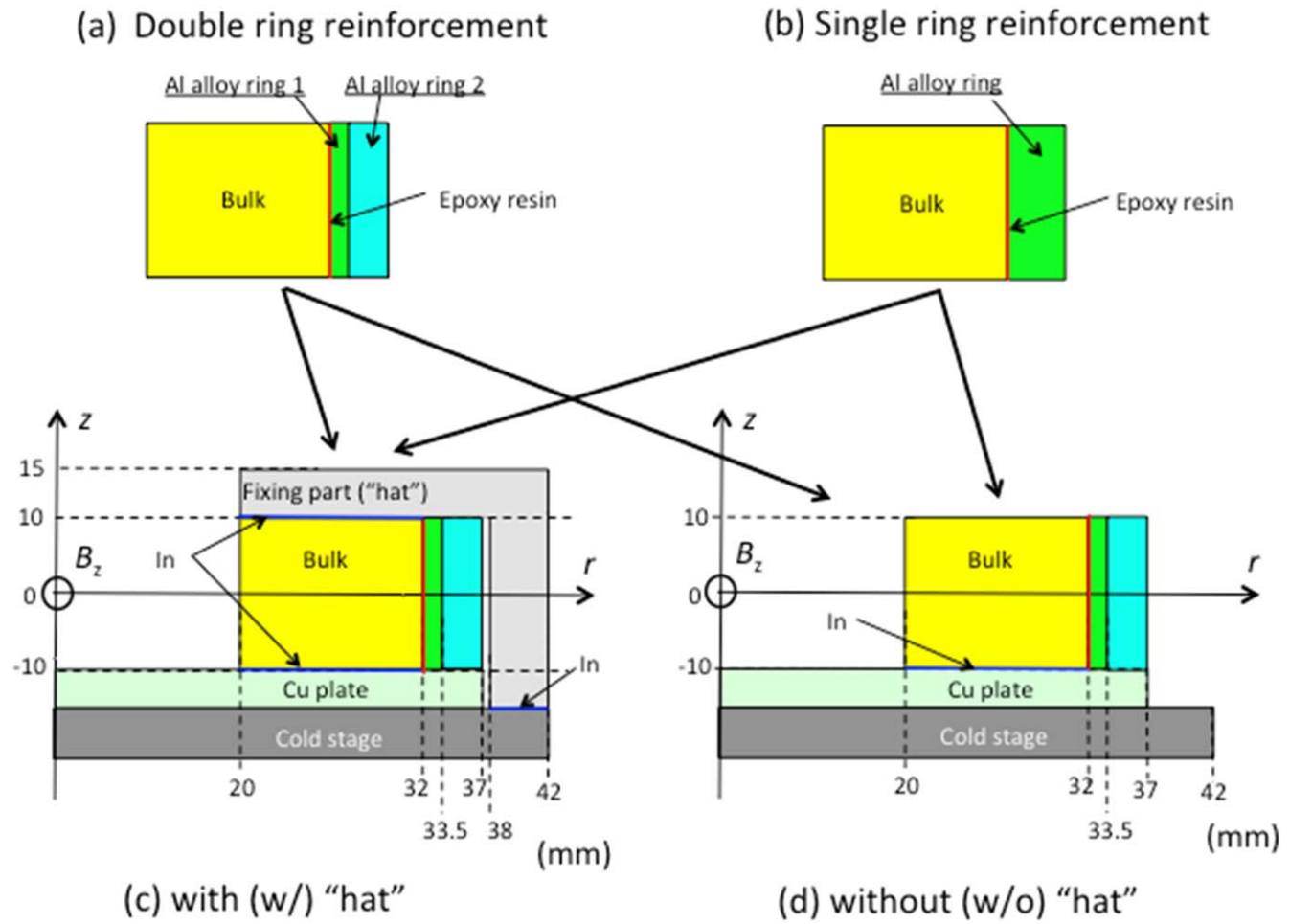

Figure 2. Cross-sectional view of the numerical model. REBaCuO ring bulk reinforced by the (a) double Al alloy ring and (b) single Al alloy ring. (c) The numerical setup during FCM for each bulk using a reinforcement hat structure to the cold stage. (d) The numerical setup during FCM for each bulk, which is fixed to the cold stage without the hat structure.

structure (74.26 mm) was 0.26 mm at 300 K; therefore, the outer Al alloy ring connects to the hat structure thermally and mechanically during the cooling process from 300 K to 50 K because the thermal shrinkage of the hat structure was greater than that of the outer Al alloy ring along the *r*-direction. In this case, the width of the Al alloy ring increased from 5 mm (initial width) to 10 mm (initial width plus the hat structure width); thus, the reinforcement effect was expected to increase [13]. To independently verify the effect of the hat structure of the upper thick plate as shown in figure 2(c), the ID of the hat structure was increased to 76.0 mm in the numerical model, which was 2 mm larger than the experimental size. In this case, the Al alloy ring did not make contact with the hat structure during the cooling process and subsequent FCM. To verify the effect of the hat structure, REBaCuO ring bulk reinforced a double ring or single ring but without the hat structure was thermally connected to a Cu plate and set on the cold stage using an In sheet, as shown in figure 2(d). A similar cooling process from 300 K to 50 K and subsequent FCM using the solenoid coil were numerically performed.

It was assumed that there was no In sheet below and above the Al alloy ring to prevent the thermal and mechanical contact of the Al alloy ring to the Cu plate and hat structure. In the experimental cooling process, the Al alloy ring shrunk significantly along the *z*-direction as well as the *r*-direction. Therefore, the absence of the In sheet below and above the Al alloy ring was reasonable assumption for reproducing the actual experimental condition.

Electromagnetic phenomena during FCM were described by fundamental equations [17, 18]. The *E*–*J* power law of the superconducting bulk was assumed to be $E = E_c(J/J_c)^n$, in which E_c ($= 10^{-4}$ V m^{-1}) is the reference electric field and n ($= 20$) is an appropriate value for a bulk superconductor [18]. The $J_c(B)$ characteristics of the ring bulk were determined using the following equation [19–21], which exhibits a fishtail shape in the magnetisation loop.

$$J_c(B) = J_{c1}\exp\left(-\frac{B}{B_L}\right) + J_{c2}\frac{B}{B_{\max}}\exp\left[\frac{1}{k}\left(1-\left(\frac{B}{B_{\max}}\right)^k\right)\right]. \quad (1)$$

Three types of $J_c(B)$ curves were examined to reproduce the experimental results of the *TS* dependence of the trapped field $B_z(r = z = 0)$. Each parameter in equation (1) for the three $J_c(B)$ curves is shown in table 1.

Table 1. Numerical parameters for the three types of $J_c(B)$ characteristics for equation (1) used in the simulation.

	J_{c1} (A m^{-2})	B_L (T)	J_{c2} (A m^{-2})	B_{max} (T)	k
Higher J_c	2.3×10^9	0.8	2.0×10^9	4.5	1.0
Best fit J_c	2.3×10^9	0.8	1.57×10^9	4.5	1.0
Lower J_c	2.3×10^9	0.8	1.3×10^9	4.5	1.0

Table 2. Mechanical parameters (Young's modulus E_Y, Poisson ratio ν, and average thermal expansion coefficient α_{av}) of the REBaCuO bulk, epoxy resin, Al alloy (A7075-T6), In and Cu used in the numerical simulation.

	E_Y (GPa)	ν	α_{av} (K^{-1})
REBaCuO bulk	100	0.33	6.80×10^{-6} [22]
Epoxy resin	3	0.37	4.61×10^{-5}
Al alloy (A7075-T6)	78	0.34	1.72×10^{-5}
In	12.7	0.45	2.78×10^{-5}
Cu	125	0.34	1.60×10^{-5}

In the numerical FCM, the ring-shaped bulk was cooled to 50 K in the magnetic field of $B_{app} = 7.3$, 8.3, and 10 T; the external field B_{ex} was then decreased linearly to 0 T at -0.222 T min^{-1} by 10 steps. The temperature variation during FCM was ignored for simplicity. The commercial FEM software package Photo-Eddy (Photon Ltd, Japan) was adapted for the analysis of the trapped field B_z.

Elastic behaviour in an isotropic material can be explained by Hooke's law, in which the stress tensor σ_{ij} is linearly proportional to the strain tensor ε_{ij}. The detailed procedure of the mechanical analysis used in this study has been shown elsewhere [12, 13]. The thermal stress under the cooling process σ_θ^{cool} from 540 K to 50 K and the total hoop stress $\sigma_\theta^{total} = \sigma_\theta^{cool} + \sigma_\theta^{FCM}$ after the cooling process and subsequent FCM at $B_{app} = 7.3$ T, 8.3 T, and 10 T were numerically simulated. The nodal force on each node of the meshed element calculated by Photo-Eddy was exported to the commercial software package Photo-ELAS (Photon Ltd, Japan) for analysis of the magnetic and thermal stresses. The mechanical parameters (Young's modulus E_Y, Poisson ratio ν, and the average thermal contraction coefficient α_{av}) of the REBaCuO ring bulk, Al alloy ring (A7075-T6), epoxy resin, In and Cu used in the elastic simulation are summarised in table 2. The α_{av} value of each material was defined as the average between 300 and 50 K, $\alpha_{av} = (L_{300} - L_{50})/L_{300}/(300 - 50)$, where L_{300} and L_{50} are the lengths of the material at 300 K and 50 K, respectively. The mechanical parameters of the REBaCuO bulk were assumed to be isotropic and homogeneous for simplicity, and typical values of the *ab*-plane were used, in which the α_{av} value was measured [22].

4. Experimental results

Figure 3(a) shows the *TS* dependence of the trapped field at the centre of the ring bulk B_z ($z = r = 0$ mm) for bulk-A without the hat structure during FCM at $B_{app} = 7.3$, 8.3, and 8.8 T at 50 K. For $B_{app} = 7.3$ and 8.3 T, B_z gradually decreased with increasing *TS*; at $TS = 10$, B_z increased with increasing B_{app}. The B_z value continued to decrease slightly after $TS = 10$ ($B_{ex} = 0$ T) due to flux creep. However, at $B_{app} = 8.8$ T, B_z suddenly dropped after $TS = 4$, and the *TS* dependence of B_z was lower than that of B_{ex}; finally, B_z reached a negative value at $TS = 10$. These results suggest that bulk-A without the hat structure was broken during FCM at $B_{app} = 8.8$ T.

Figure 3(b) shows the *TS* dependence of B_z ($z = r = 0$ mm) for bulk-B with the hat structure during FCM at $B_{app} = 7.3$, 8.3, 8.8, 9.4 T, and 10 T at 50 K. The B_z value gradually decreased with increasing *TS* for each B_{app}. The value of B_z at $B_{app} = 8.3$ T was larger than that at $B_{app} = 7.3$ T. However, the final B_z value at $TS = 10$ with a B_{app} higher than 8.3 T was nearly identical, which suggests that the ring bulk was fully magnetised at $B_{app} \geqslant 8.3$ T; therefore, a supercurrent as large as $J_c(B)$ flowed in all of the ring bulk area. It should be noted that a B_z value of 6.8 T was trapped at the centre of bulk-B without fracture. These results suggest that the hat structure is effective for achieving higher trapped fields without fracture compared with the results of bulk-A without the hat structure, as shown in figure 3(a). However, the ID and ht values of bulk-A and bulk-B are different from one another; therefore, this is not necessarily an exact comparison between identical cases with and without the hat structure. A detailed discussion is given in a later section.

Figure 3(c) shows the *TS* dependence of the temperature change for bulk-B with the hat structure during FCM at a B_{app} of up to 10 T at 50 K. The temperature increased with increasing *TS* at each B_{app}, and the temperature rise stopped around $TS = 10$; this is when the magnetic flux movement driven by the Lorentz force $F_L = J_c \times B$ against the pinning force F_p stopped. Therefore, the cooling power of the cryogenic refrigerator was stronger than the heat generation. As a result, the maximum temperature rise was as small as 1.5 K on the upper surface of the hat structure for FCM at $B_{app} = 10$ T.

Figure 3(d) shows the temperature dependence of the trapped field B_z ($z = r = 0$ mm) at the centre of bulk-B after FCM was performed at 50 K for each B_{app}. The B_z versus T curve for $B_{app} = 7.3$ T was lower than that of other B_{app} at $T < 55$ K; however, the curves above 55 K were identical for each B_{app}, which is closely reflected in the results of figure 3(b).

5. Numerical simulation results for double Al ring reinforcement

5.1. Determination of average $J_c(B)$ for bulk-B

Electromagnetic and mechanical properties strongly depend on the $J_c(B, T)$ characteristics of the superconducting bulk. To precisely estimate the hoop stress in the ring bulk during FCM using simulation, it is necessary to determine the

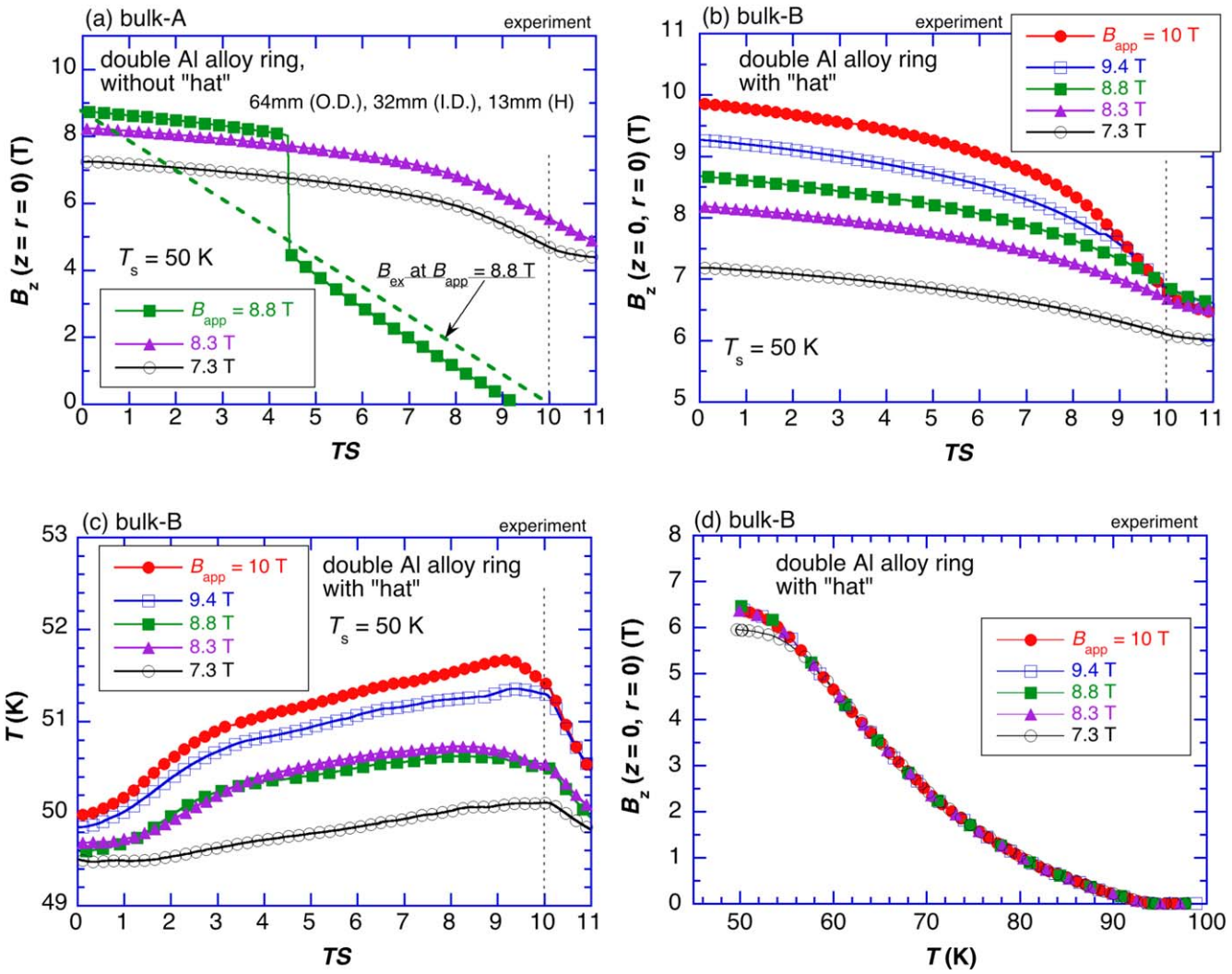

Figure 3. (a) *TS* dependence of the trapped field $B_z(z = r = 0)$ at the centre of (a) bulk-A without the hat structure and (b) bulk-B with the hat structure during FCM at various B_{app} at 50 K. (c) *TS* dependence of the temperature, *T*, on the hat structure above the bulk-B during FCM at various B_{app} at 50 K. (d) Temperature dependence of the trapped field, $B_z(z = r = 0\,\text{mm})$, at the centre of the bulk-B, after the FCM procedure was performed at 50 K for each B_{app}.

$J_c(B, T)$ characteristics of the bulk; this is because the stress is closely related to the Lorentz force F_L. In a previous simulation paper [23], the $J_c(B)$ characteristics, which were estimated by the magnetic moment hysteresis (*M–H*) loop using a small piece cut from the bulk, were typically used. Bean's critical state model [24] or the Kim model [25] were also used. Since the $J_c(B)$ determined by the *M–H* loop occasionally overestimates the trapped field by FCM, $J_c(B)$ had to be adjusted to one third of its small specimen value to adequately reproduce the FCM results [21]. In this study, a new method has been proposed to estimate the average $J_c(B)$ characteristics of the bulk, in which the *TS* dependence of $B_z(z = r = 0\,\text{mm})$ measured experimentally was fitted using the $J_c(B)$ characteristics shown in equation (1).

Figure 4(a) shows the numerical simulation results of *TS* dependence of $B_z(z = r = 0\,\text{mm})$ during FCM at $B_{app} = 10\,\text{T}$ at 50 K for the three $J_c(B)$ curves shown in table 1; these results were compared to the experimental result. The three $J_c(B)$ curves are shown in the inset. It was found that the numerical result using the *best fit* J_c well reproduced the experimental curve, compared to the cases for lower and higher J_c. Figure 4(b) shows the numerical simulation results of the *TS* dependence of $B_z(z = r = 0\,\text{mm})$ during FCM at $B_{app} = 7.3$, 8.3, and 10 T at 50 K, in which the best fit J_c was used; these results were also compared with the experimental results. The parameters used in the best fit J_c reproduced the experimental curves for FCM with different B_{app} values. This suggests that the *average* $J_c(B)$ characteristics can be estimated using this method, which produces reasonable values for a typical REBaCuO bulk at 50 K [21, 23], even though the $J_c(B)$ characteristics cannot be determined uniquely. In a later section, the numerical simulation results of the hoop stress during FCM are estimated using the best fit J_c characteristics.

5.2. Shrink-fit effect of the outer Al alloy ring from 540 K to 300 K

In this subsection, the mechanical reinforcement effect of a double ring structure was investigated using numerical

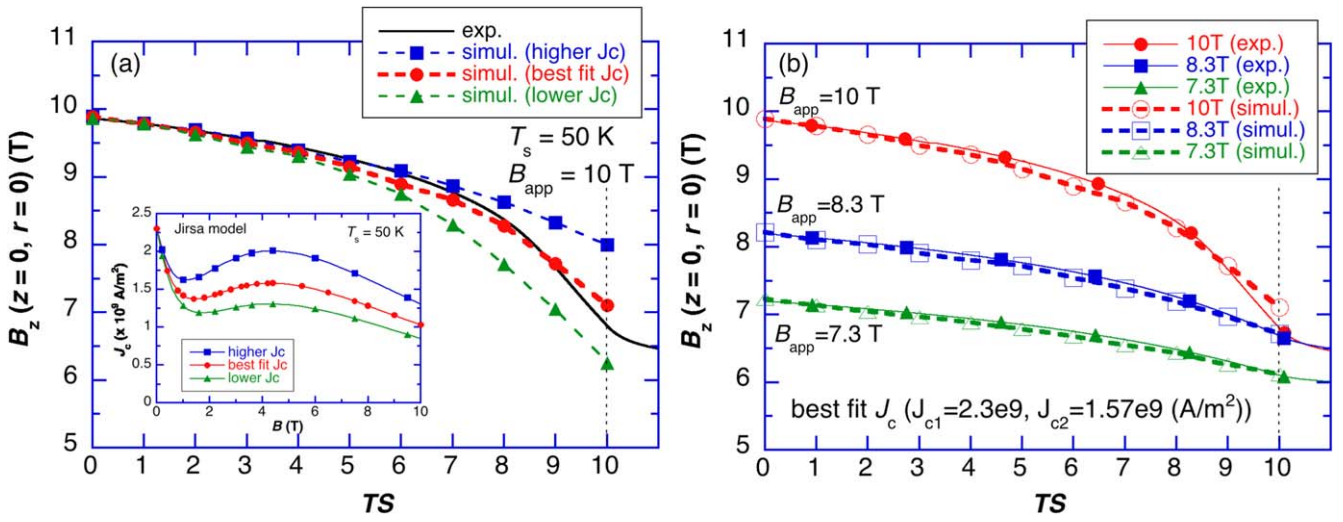

Figure 4. (a) The numerical results of *TS* dependence of $B_z(z = r = 0\,\text{mm})$ during FCM at $B_{app} = 10\,\text{T}$ at 50 K for three $J_c(B)$ curves shown in table 1, compared to that the experimental result which was recited from figure 3(b). Three $J_c(B)$ curves at 50 K are shown in the inset. (b) The numerical results of the *TS* dependence of $B_z(z = r = 0\,\text{mm})$ during FCM at $B_{app} = 7.3\,\text{T}$, 8.3 T and 10 T at 50 K using the best fit J_c, compared to the experimental results.

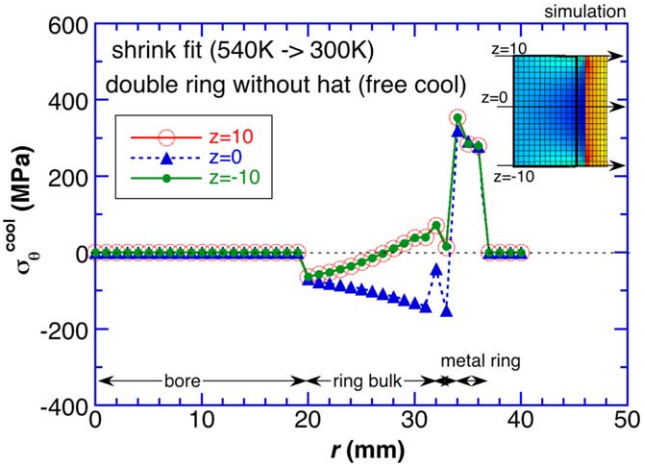

Figure 5. The radius (r) dependence of the thermal hoop stress, $\sigma_\theta^{\text{cool}}$, at each z-position for the ring bulk reinforced by the double Al alloy ring, in which the outer Al ring was shrink-fitted from 540 K to 300 K.

simulation. Figure 5 shows the radius (r) dependence of the thermal hoop stress $\sigma_\theta^{\text{cool}}$ at the bulk centre ($z = 0\,\text{mm}$) and the bulk surface ($z = \pm 10\,\text{mm}$) for ring bulk reinforced by a double Al alloy ring; the outer Al alloy ring (Al alloy ring 2) was heated to 540 K, fitted to the inner Al alloy ring (Al alloy ring 1), and then cooled to 300 K. For the bulk centre ($z = 0\,\text{mm}$), a compressive stress greater than $-100\,\text{MPa}$ was applied to the ring bulk ($20\,\text{mm} < r < 32\,\text{mm}$); for the bulk surface ($z = \pm 10\,\text{mm}$), a tensile stress of up to $+75\,\text{MPa}$ was applied to the outer region of the ring bulk because of the larger thermal contraction of the Al alloy ring along the z-direction as well as the r-direction [12]. These results suggest that the compressive stress is enhanced by the double ring structure at the bulk centre ($z = 0\,\text{mm}$), but is weakened at the bulk surface; this is compared to ring bulk reinforced by a single ring, where the stress is not applied to the ring bulk at 300 K.

5.3. Overall shrink-fit effect from 540 K to 50 K

The ring bulk reinforced by the double Al alloy ring was set on the cold stage with and without the hat structure at 300 K and then cooled to 50 K. Figures 6(a) and (b) show the simulation results of the radius (r) dependence of the total thermal hoop stress $\sigma_\theta^{\text{cool}}$ for the ring bulk with and without the hat structure, respectively, at the bulk centre ($z = 0\,\text{mm}$) and the bulk surface ($z = \pm 10\,\text{mm}$); the outer ring was cooled from 540 K to 50 K, and the inner ring was cooled from 300 K to 50 K. For the case with the hat structure as shown in figure 6(a), a large compressive stress was applied over the bulk area; the compressive stress gradually decreased from the bottom surface to the top surface. For the case without the hat structure as shown in figure 6(b), a larger tensile stress was applied at the top surface ($z = +10\,\text{mm}$), compared to that of the shrink-fit from 540 K to 300 K shown in figure 5. At the bulk centre ($z = 0\,\text{mm}$) and the bottom surface ($z = -10\,\text{mm}$), a large compressive stress was applied during the overall shrink fitting process from 540 K to 50 K. The inhomogeneous thermal stress for the double alloy ring reinforcement without the hat structure, which introduced a shear stress to the ring bulk, might affect the bulk failure only during cooling. If this shear stress were applied in the bulk, the bulk could peel along the c-direction; this is because the fracture strength along the c-axis is about one order of magnitude smaller than that of the ab-plane [26, 27].

5.4. Total hoop stress σ_θ^{total} during the cooling process and FCM ($B_{app} = 8.3\,\text{T}$)

Figure 7 shows the *TS* dependence of the cross-sectional profiles of total hoop stress $\sigma_\theta^{\text{total}}$ ($= \sigma_\theta^{\text{cool}} + \sigma_\theta^{\text{FCM}}$) at the (a) top surface ($z = +10\,\text{mm}$) and (b) bulk centre ($z = 0\,\text{mm}$) of the ring bulk reinforced by the double Al alloy ring with the hat structure during FCM at $B_{app} = 8.3\,\text{T}$. Similar plots of $\sigma_\theta^{\text{total}}$ at the (c) top surface ($z = +10\,\text{mm}$) and (d) bulk centre

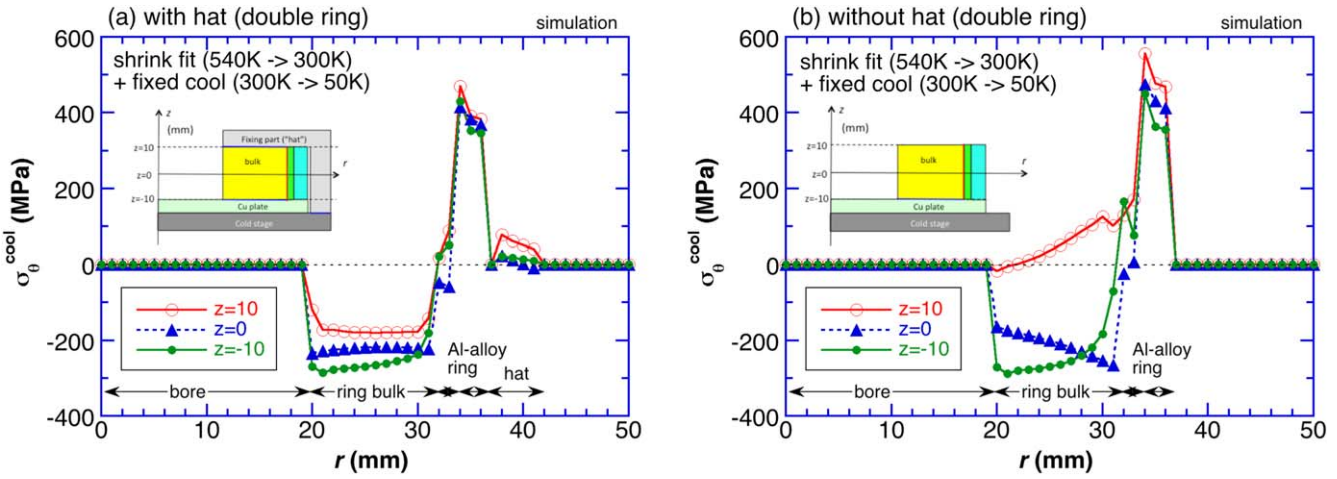

Figure 6. The radius (r) dependence of the total thermal hoop stress, σ_θ^{cool}, for the ring bulk reinforced by double Al ring (a) with and (b) without the hat structure at the bulk centre ($z = 0$ mm) and bulk surface ($z = \pm 10$ mm), in which the outer Al alloy ring was cooled from 540 K to 50 K and then the bulk module was cooled from 300 K to 50 K.

($z = 0$ mm) of the ring bulk reinforced by the double Al alloy ring without the hat structure are also shown. In each case, the σ_θ^{total} profile at the 0 step was recited from figure 6. The σ_θ^{total} value at each position within the ring bulk region gradually increased along the positive (tensile) direction with increasing *TS* due to the increase in the electromagnetic hoop stress; then σ_θ^{total} slightly decreased with further increase of *TS*. A distinctive difference in the σ_θ^{total} profile between the case with and without the hat structure was seen at the bulk surface (z = +10 mm). For the case without the hat structure as shown in figure 7(c), the σ_θ^{total} value was +160 MPa at $r = 20$ mm and +195 MPa at $r = 31$ mm for $TS = 6$, which was fairly larger than the fracture strength (50–70 MPa) of a typical Ag-doped REBaCuO bulk [26–28]. Therefore, the ring-shaped bulk might break, even if the ring bulk were reinforced with the double Al alloy ring. In the experiment with bulk-A, as shown in figure 3(a), bulk-A actually broke after $TS = 4$ of FCM at $B_{app} = 8.8$ T. For the case with the hat structure shown in figure 7(a), the maximum σ_θ^{total} was −100 MPa (compressive) on the bulk surface, which suggests that the ring bulk might not break, as shown in figure 3(b). At the bulk centre ($z = 0$ mm), as shown in figures 7(b) and (d), the compressive stress could be safely applied to the ring-shaped bulk with and without the hat structure during the cooling process and FCM.

The hat structure may be similar to a *Yoroi-coil structure*, which has been proposed for reinforcement of the pancake coil wound by REBaCuO tape on the Hastelloy substrate, so that it may withstand the electromagnetic hoop stress [29, 30]. The outer plates made of glass fibre reinforced plastics (GFRP) or carbon fibre reinforced plastics (CFRP) in the Yoroi-coil structure exist on the pancake coil. However, there is no shrink-fit effect in the reinforcing outer plates, because the thermal expansion coefficient of GFRP and CFRP is much smaller than that of the Hastelloy substrate. The hat structure especially demonstrates this important effect during the cooling process by reducing the inhomogeneous compressive stress at the bulk surface. In addition, the reinforcement effect for the electromagnetic hoop stress is also enhanced by the hat structure.

Figures 8(a) and (b) summarise the *TS* dependence of σ_θ^{total} at typical positions of the ring bulk with and without the hat structure, respectively, during FCM at $B_{app} = 8.3$ T. The σ_θ^{total} value at each position increased with increasing *TS*, reached a maximum at around $TS = 6$, and then decreased with the increase in *TS*. The maximum σ_θ^{total} value was observed at the outer and top surface ($z = 10$ mm, $r = 31$ mm), which was +28 MPa for the ring bulk with the hat structure and +200 MPa for the ring bulk without the hat structure. Therefore, the fracture of bulk-A during FCM at $B_{app} = 8.8$ T as shown in figure 3(a) can be understood qualitatively from these simulation results; however, σ_θ^{total} of bulk-A may be slightly smaller than that of bulk-B because of the smaller height of bulk-A (ht = 13 mm).

6. Numerical simulation results of ring bulk reinforced by a single Al alloy ring

6.1. Shrink-fit effect from 300 K to 50 K

In section 4, the ring bulk reinforced by the double Al alloy ring and the hat structure was successfully magnetised at $B_{app} = 10$ T, implying that both the double ring and hat structure might simultaneously contribute the success. To analyse the double ring effect independently, the hoop stresses during the cooling process and FCM were numerically investigated for ring bulk reinforced by a *single Al alloy ring*, as shown in figure 2(d).

Figure 9 shows the simulation results of the radius (r) dependence of the thermal hoop stress σ_θ^{cool} at the bulk centre ($z = 0$ mm) and the top and bottom surfaces of the bulk ($z = \pm 10$ mm) for ring bulk reinforced by a single Al alloy ring with the hat structure; it was then cooled from 300 to 50 K. The compressive stress in the ring bulk region was reduced relative to that in the case of the double Al alloy ring, as shown in figure 6(a). For example, at the position ($z = 0$

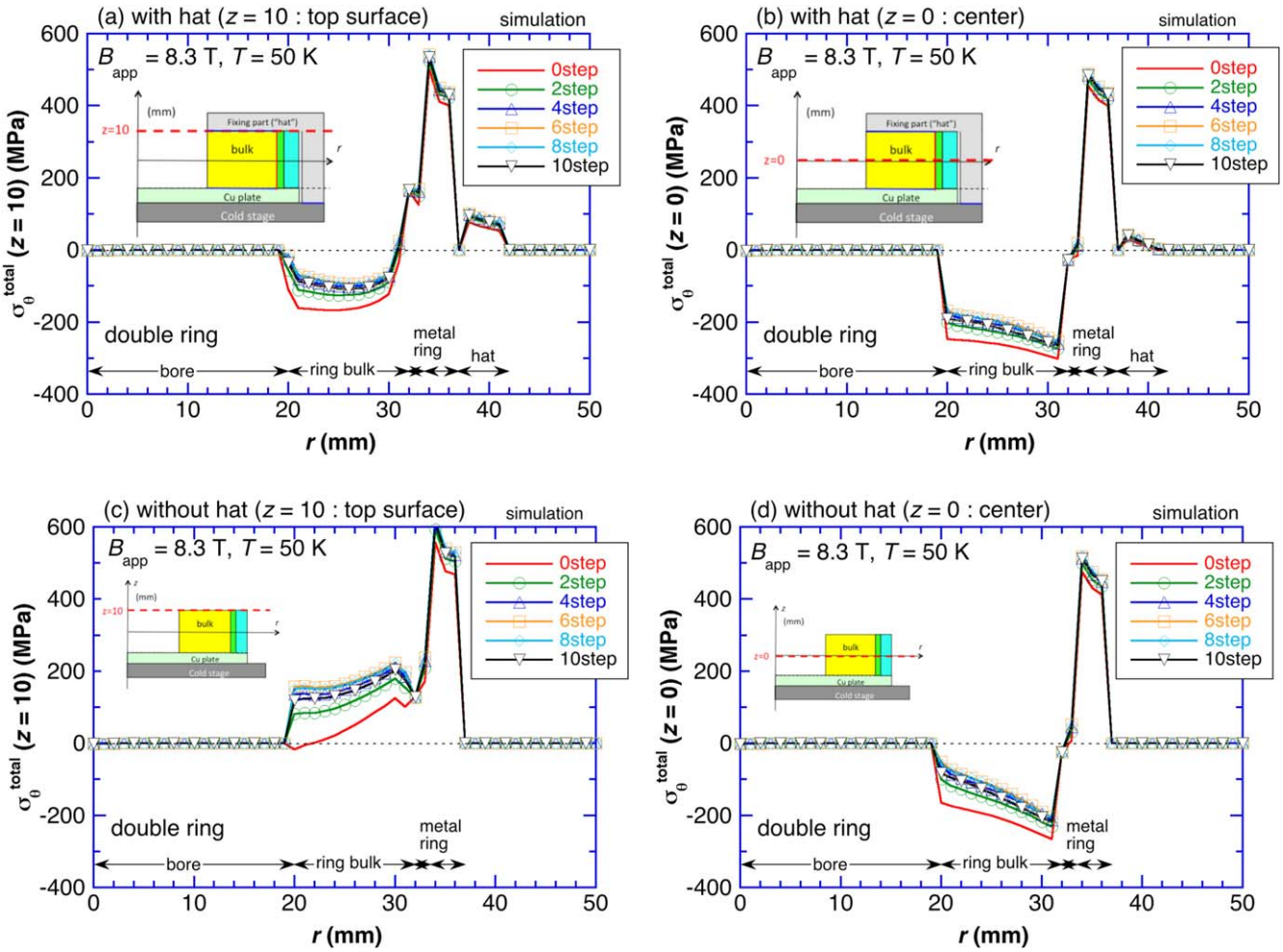

Figure 7. Time step (*TS*) dependence of the cross-sectional profiles of total hoop stress, $\sigma_\theta^{\text{total}}$ ($= \sigma_\theta^{\text{cool}} + \sigma_\theta^{\text{FCM}}$), at (a) top surface ($z = +10$ mm) and (b) bulk centre ($z = 0$ mm) of the ring bulk with the hat structure during FCM at $B_{\text{app}} = 8.3$ T. The similar profiles of $\sigma_\theta^{\text{total}}$ at (c) top surface ($z = +10$ mm) and (d) bulk centre ($z = 0$ mm) of the ring bulk without the hat structure during FCM at $B_{\text{app}} = 8.3$ T are also shown.

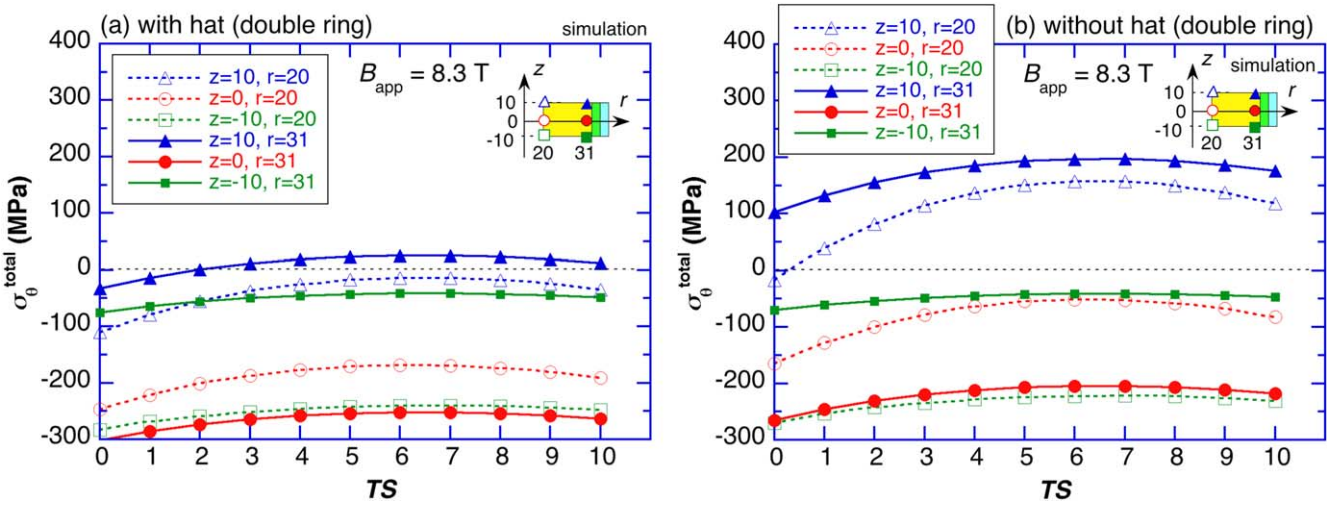

Figure 8. *TS* dependence of the $\sigma_\theta^{\text{total}}$ value at the typical positions of the ring bulk (a) with and (b) without the hat structure during FCM at $B_{\text{app}} = 8.3$ T.

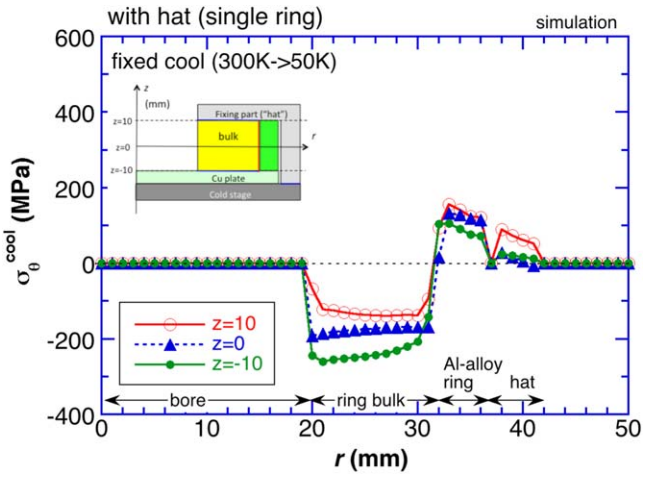

Figure 9. The simulation results of the radius (r) dependence of the thermal hoop stress, σ_θ^{cool}, for the ring bulk reinforced by single Al alloy ring with the hat structure at the bulk centre ($z = 0$ mm) and the top and bottom surfaces of the bulk ($z = \pm 10$ mm) during cooling from 300 K to 50 K.

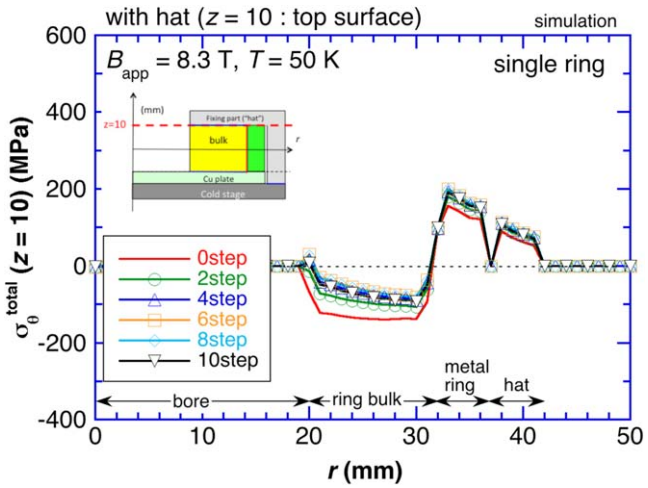

Figure 10. *TS* dependence of the cross-sectional plots of total hoop stress, σ_θ^{total} ($= \sigma_\theta^{cool} + \sigma_\theta^{FCM}$), at the top surface ($z = 10$ mm) of the ring bulk reinforced by single Al alloy ring with the hat structure during FCM at $B_{app} = 8.3$ T.

and $r = 25$ mm), the compressive σ_θ^{cool} was slightly reduced from -250 MPa for the double ring to -180 MPa for the single ring. However, a large compressive thermal stress was still applied throughout the ring bulk region during the cooling process by the hat structure, even when the single Al alloy ring was used.

6.2. Total hoop stress σ_θ^{total} during the cooling process and FCM ($B_{app} = 8.3$ T)

Figure 10 shows the *TS* dependence of the cross-sectional profiles of total hoop stress σ_θ^{total} ($= \sigma_\theta^{cool} + \sigma_\theta^{FCM}$) at the top surface ($z = +10$ mm) of the ring bulk reinforced by a single Al alloy ring with the hat structure during FCM at $B_{app} = 8.3$ T. The σ_θ^{total} in the ring bulk was the compressive stress and slightly changed along the positive (tensile) direction with increasing *TS* due to the increase in the electromagnetic hoop stress. Similar σ_θ^{total} behaviour with the double Al alloy ring can be seen in figure 7(a). These results suggest that the double Al alloy ring has a limited effect and that the hat structure is the most effective for applying the compressive stress needed to avoid fracture during FCM.

Figure 11 shows the *TS* dependence of σ_θ^{total} at typical positions of the ring bulk reinforced by a single Al alloy ring with the hat structure during FCM at $B_{app} = 8.3$ T, which was extracted from figure 10. The σ_θ^{total} value at each position increased with increasing *TS*, reached a maximum at approximately $TS = 6 \sim 7$, and then decreased with increasing *TS*. A maximum σ_θ^{total} of $+28$ MPa was seen at the inner top ring bulk surface ($z = 10$ mm, $r = 20$ mm), which was slightly larger than that of the bulk reinforced by the double Al alloy ring, as shown in figure 8(a). The maximum σ_θ^{total} was not determined by the structure of the Al alloy ring, but was primarily governed by the existence of the hat structure.

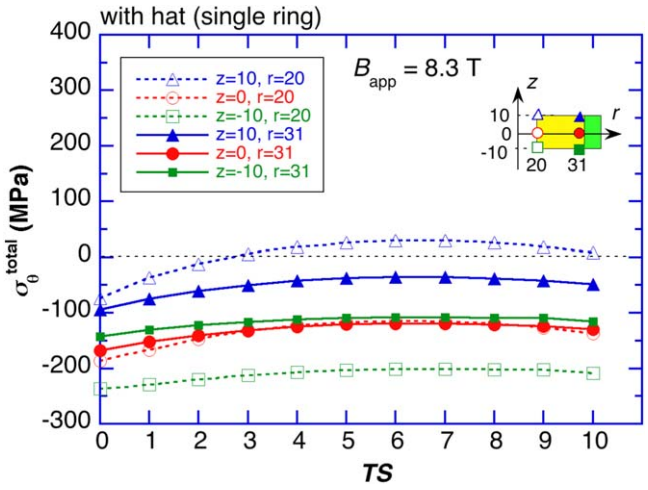

Figure 11. *TS* dependence of the σ_θ^{total} value at the typical positions of the ring bulk reinforced by single Al alloy ring with the hat structure during FCM at $B_{app} = 8.3$ T.

7. Optimal reinforcement structure for ring bulk

In the final section, we summarise the mechanical reinforcement effects of the double and single Al alloy rings with the hat structure during FCM, as shown in sections 5 and 6. We also overview the optimal and practical reinforcement structure for REBaCuO ring-shaped bulk, including our previous investigations.

Figures 12(a) and (b) show the results of the numerical simulation of the maximum σ_θ^{total} value, σ_θ^{total}(max), at typical positions in the ring bulk with and without the hat structure, respectively, as a function of B_{app} during FCM. The results for the ring bulk reinforced by only the double or single Al alloy ring are also shown. The σ_θ^{total}(max) value at each position linearly increased with increasing B_{app} for all cases. In the experimental setup similar to the conditions shown in figure 12(a), a σ_θ^{total}(max) of $+50$ MPa was applied at the periphery of the bulk surface ($z = 10$ mm, $r = 31$ mm) at

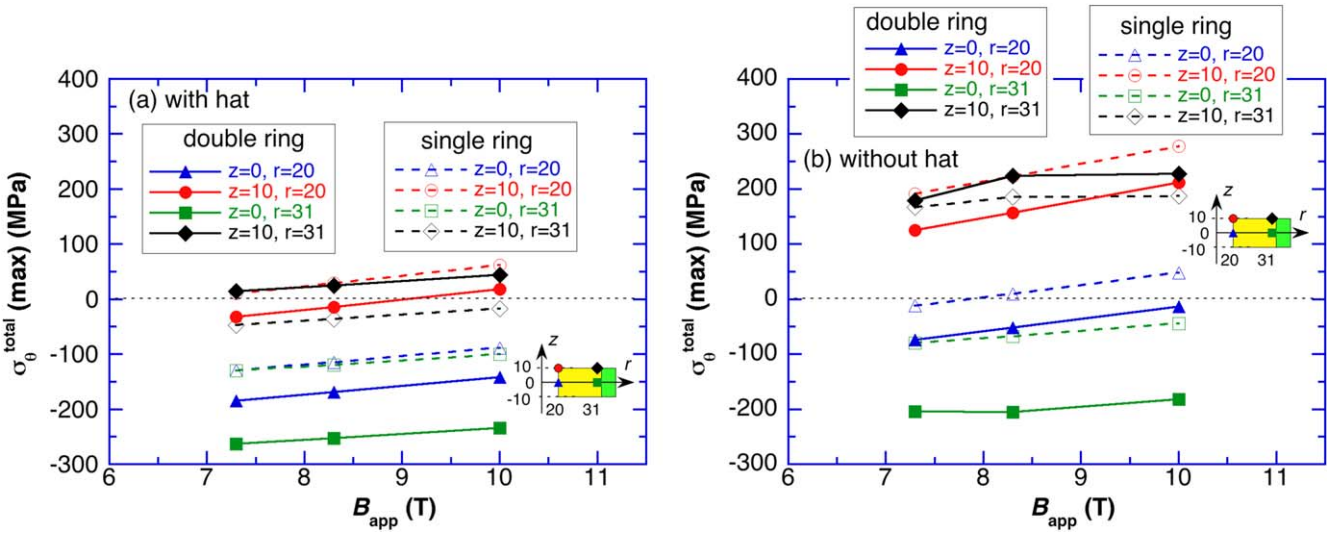

Figure 12. The numerical simulation results of the σ_θ^{total}(max) value at the typical positions in the ring bulk reinforced by the double and single Al alloy ring (a) with and (b) without the hat structure, as a function of the applied magnetic field, B_{app}, during FCM.

$B_{app} = 10$ T, which is smaller than the fracture strength of a typical Ag-doped REBaCuO bulk [26–28]. The σ_θ^{total}(max) at other positions was a large negative (compressive) or slightly positive (tensile) value. For the case using a single Al alloy ring with the hat structure, a σ_θ^{total}(max) of +65 MPa was applied at the innermost position of the bulk surface ($z = 10$ mm, $r = 20$ mm) at $B_{app} = 10$ T, which was slightly larger than that for the double Al alloy ring case. These results suggest that for both double and single Al alloy ring reinforcement with the hat structure, the ring bulk would not break at a B_{app} up to 10 T.

As for single and double Al alloy ring reinforcement without the hat structure as shown in figure 12(b), σ_θ^{total}(max) exceeded +200 MPa at $B_{app} = 10$ T; this suggests that the σ_θ^{total}(max) value was larger than the fracture strength [26–28]. These results indicate that the hat structure effectively reinforced the ring bulk, but the mechanical reinforcement effect of the double Al alloy ring was limited, even when the inner surface of the hat structure did not make contact with the outer surface of the double Al alloy ring after the cooling process, as explained in the section 3. If the hat structure contacts the double Al alloy ring after the cooling process, the width of the Al alloy ring would effectively increase by 5 mm, thus increasing width reinforcement effect of the Al alloy ring. Combining the Al alloy ring width reinforcement effect with the reinforcement effect of the hat structure [14], the compressive stress becomes large and the ring bulk can be magnetised more safely. Therefore, the ring bulk reinforced by a double Al alloy ring and hat structure and set on the cold stage of a cryogenic refrigerator can be cooled to 50 K and magnetised under a magnetic field up to 10 T without fracture; this correlates reasonably well with the experimental results.

We have determined the optimal reinforcement structure that can prevent mechanical fracture for REBaCuO ring bulk during FCM with an applied magnetic field up to 10 T. We have also investigated the mechanical reinforcement effect of a metal ring on REBaCuO ring bulk during FCM. The reinforcement enhancement of increasing the width of the metal ring was found to be effective [14]. Although SUS316 is better than Al alloy as a reinforcement ring material due to larger Young's modulus [14], the non-magnetic Al alloy (A7075-T6) ring must be used for the NMR bulk magnet. The hat structure was found to be effective, as shown in this study and in [15]; however, the double ring effect was limited. The hoop stress and reinforcement effect also change depending on the ID, OD and ht of the ring bulk with identical $J_c(B)$ [31]. Therefore, we can conclude that the proposed hat structure is the most reliable and effective reinforcement structure to realise a 400 MHz (9.4 T) NMR bulk magnet system.

8. Conclusion

We have experimentally and numerically investigated a new reinforcement hat structure for the ring-shaped REBaCuO bulk superconductor, which was shrink-fitted by a double Al alloy ring and set on the cold stage of a cryogenic refrigerator prior to FCM. The important results and conclusions in this study are summarised as follows.

(1) In the experiments, the ring bulk (64 mm OD, 40 mm ID and 20 mm ht) with the hat structure trapped a magnetic field as high as 6.8 T at 50 K during FCM at $B_{app} = 10$ T without fracture; a similar ring bulk (64 mm OD, 32 mm ID and 13 mm ht) without the hat structure broke during FCM at $B_{app} = 8.8$ T.
(2) The magnetic field dependence of the average critical current density $J_c(B)$ was experimentally determined by the results of *TS* dependence of the trapped field B_z at the centre of the ring bulk; this is one of the practical methods for estimating $J_c(B)$ for the numerical

simulation of the mechanical properties of the bulk. Using numerical simulation, the total hoop stress $\sigma_\theta^{\text{total}}$ ($= \sigma_\theta^{\text{cool}} + \sigma_\theta^{\text{FCM}}$) in the bulk reinforced by the double Al alloy ring and hat structure was analysed during FCM with a B_{app} of up to 10 T after cooling to 50 K; the maximum $\sigma_\theta^{\text{total}}$ was lower than the typical fracture strength of the REBaCuO bulk (50–70 MPa). Therefore, the results of the simulation verify the experimental FCM results at $B_{\text{app}} = 10$ T.

(3) The effect of the hat structure on mechanical reinforcement was verified using numerical simulation and compared with the case without the hat structure, in which the thermal compressive stress $\sigma_\theta^{\text{cool}}$ provides the greatest contribution for preventing mechanical fracture.

(4) The effect of the double Al alloy ring reinforcement was compared with that of the conventional single Al alloy ring using numerical simulation. The double ring effect was limited, and the reinforcement method with the hat structure was fairly effective in reducing the hoop stress for the ring bulk during FCM at $B_{\text{app}} = 10$ T without fracture. These results suggest that it is possible to realise a 400 MHz (9.4 T) NMR bulk magnet system.

Acknowledgments

This research is partially supported by Development of Systems and Technologies for Advanced Measurement and Analysis from the Japan Agency for Medical Research and Development (AMED) and by JSPS KAKENHI Grant No. JP15K04646. The authors would also like to thank Dr Mark D Ainslie of the University of Cambridge for his valuable suggestions about the numerical simulation of the mechanical properties.

ORCID iDs

H Fujishiro https://orcid.org/0000-0003-1483-835X
T Naito https://orcid.org/0000-0001-7594-3466

References

[1] Tomita M and Murakami M 2003 *Nature* **421** 517–20
[2] Gruss S, Fuchs G, Krabbes G, Verges P, Stover G, Muller K-H and Fink J 2001 *Appl. Phys. Lett.* **79** 3131
[3] Durrell J H *et al* 2014 *Supercond. Sci. Technol.* **27** 082001
[4] Nakamura T, Itoh Y, Yoshikawa M, Oka T and Uzawa J 2007 *Concepts Magn. Reson.* B **31B** 65–70
[5] Nakamura T, Tamada D, Yanagi Y, Itoh Y, Nemoto T, Utsumi H and Kose K 2015 *J. Magn. Reson.* **259** 68–75
[6] Ogawa K, Nakamura T, Terada Y, Kose K and Haishi T 2011 *Appl. Phys. Lett.* **98** 234101
[7] Ren Y, Weinstein R, Liu J, Sawh R P and Foster C 1995 *Physica* C **251** 15–26
[8] Johansen T, Wang C, Chen Q Y and Chu W–K 2000 *J. Appl. Phys.* **88** 2730–3
[9] Johansen T 2000 *Supercond. Sci. Technol.* **13** R121–37
[10] Huang C, Yong H and Zhou H 2013 *Supercond. Sci. Technol.* **26** 105007
[11] Johansen T H, Chen Q Y and Chu W-K 2001 *Physica* C **349** 201–10
[12] Fujishiro H, Ainslie M D, Takahashi K, Naito T, Yanagi Y, Itoh Y and Nakamura T 2017 *Supercond. Sci. Technol.* **30** 085008
[13] Takahashi K, Fujishiro H, Naito T, Yanagi Y, Itoh Y and Nakamura T 2017 *Supercond. Sci. Technol.* **30** 115006
[14] Takahashi K, Fujishiro H, Naito T, Yanagi Y, Itoh Y and Nakamura T 2018 *IEEE Trans. Appl. Supercond.* **28** 6800705
[15] Fujishiro H, Takahashi K, Naito T, Yanagi Y, Itoh Y and Nakamura T 2018 *Physica* C **550** 52
[16] Takahashi K, Namba S, Fujishiro H, Naito T, Yanagi Y, Itoh Y and Nakamura T 2019 *Supercond. Sci. Technol.* **32** 015007
[17] Fujishiro H, Itoh Y, Yanagi Y and Nakamura T 2015 *Supercond. Sci. Technol.* **28** 095018
[18] Ainslie M D and Fujishiro H 2015 *Supercond. Sci. Technol.* **28** 053002
[19] Muralidhar M, Sakai N, Jirsa M, Koshizuka N and Murakami M 2004 *Appl. Phys. Lett.* **85** 3504
[20] Jirsa M, Půst L, Dlouhý D and Koblischka M R 1997 *Phys. Rev.* B **55** 3276–84
[21] Ainslie M D, Fujishiro H, Mochizuki H, Takahashi K, Shi Y-H, Namburi D K, Zhou D, Dennis A R and Cardwell D A 2016 *Supercond. Sci. Technol.* **29** 074003
[22] Naito T, Mochizuki H, Fujishiro H and Teshima H 2016 *Supercond. Sci. Technol.* **29** 034005
[23] Kii T *et al* 2012 *IEEE Trans. Appl. Supercond.* **22** 4100904
[24] Bean C P 1962 *Phys. Rev. Lett.* **8** 250
[25] Kim Y B, Hempstead C F and Stmad A R 1965 *Phys. Rev.* **139** A1163
[26] Lee D and Salama K 1990 *Japan. J. Appl. Phys.* **29** L2017–9
[27] Matsui M, Sakai N and Murakami M 2002 *Supercond. Sci. Technol.* **15** 1092–8
[28] Katagiri K, Murakami A, Kan R, Kasaba K, Noto K, Muralidhar M, Sakai N and Murakami M 2003 *Physica* C **392–396** 526–30
[29] Nagaya S, Watanabe T, Tamada T, Naruse M, Kashima N, Katagiri T, Hirano N, Awaji S, Oguro H and Ishiyama A 2013 *IEEE Trans. Appl. Supercond.* **23** 4601204
[30] Watanabe T *et al* 2015 *IEEE Trans. Appl. Supercond.* **25** 8400204
[31] Fujishiro H, Takahashi K, Naito T, Yanagi Y, Itoh Y, Nakamura T and Ainslie M D 2019 *IEEE Trans. Appl. Supercond.* **29** 6801206